Hindawi
Geofluids
Volume 2022, Article ID 7447423, 11 pages
https://doi.org/10.1155/2022/7447423

Research Article

Head-On Dynamic Manifestations in the Roadway Driving with Small Coal Pillar under the Influence of Roof Drainage: A Case Study from Uxin Banner

Yunhai Cheng,[1] **Fenghui Li**,[2] **Xiufeng Zhang**,[3] **Chao Wang**,[4] **and Gangwei Li**[2]

[1]*National Engineering Laboratory of Coalmine Backfilling Mining, Shandong University of Science and Technology, Taian 271000, China*
[2]*School of Mining Engineering, Anhui University of Science and Technology, Huainan 232000, China*
[3]*Coal Burst Prevention and Control Research Centre, Shandong Energy Group Co., Ltd., Jinan 250000, China*
[4]*Yankuang Energy Group Co., Ltd., Zoucheng 273500, China*

Correspondence should be addressed to Fenghui Li; ahlifenghui@163.com

Received 3 April 2022; Revised 27 July 2022; Accepted 2 August 2022; Published 23 August 2022

Academic Editor: Yang Yu

In the Uxin Banner area of the Inner Mongolia Autonomous Region, mines that have experienced rock bursts have all been affected by the presence of confined water in the roof strata. Strong mine pressure appears in the working face with about 30 m wide coal pillar in this area, and the research and practice of prevention and control of rock burst by small coal pillar are carried out. Mining-related events linked to the preservation of small coal pillars in the 2-2 coal seam of this region, and studies of the phenomenon, have shown that head-on rock bursts occur during gob-side roadway driving at the edge of the drained area, making it necessary to identify the sources of pressure triggering the events, to determine the related threshold criteria, and to identify methods to reduce the occurrence and magnitude of the rock burst events. This study used the gob-side entry driving in the drained area of the 2202 auxiliary haulage roadway of a mine as a case study. The paper built a structural and computational model for overburdens (including the drained stratum) before mining disturbance, based on the theory for a continuously distributed Winkler elastic foundation. The models used and developed in our study were used to identify, quantify, and describe the changes to stress and the transfer of stress during the drainage process. On the basis of the effects of drainage stress induced by the gob-side entry driving, we outlined a method for ranking the level of rock burst hazard associated with the areas in and adjacent to the drained area. The level of rock burst hazard associated with the entry driving could be arranged in descending order as follows: parallel boundary > vertical boundary > undrained area > drained area. Stress threshold criteria for head-on ejection were also proposed in the paper, namely, (1) the occurrence (or not) of coal ejection during loading and (2) the critical stress for the occurrence of ejection. Field monitoring indicated that microseismic events and energy are mainly concentrated in the driving region parallel to the boundary of the drained area. We concluded that head-on large-diameter borehole destressing would effectively reduce the likelihood of a rock burst occurrence.

1. Introduction

All mines susceptible to rock bursts in the Uxin Banner area of the Inner Mongolia Autonomous Region (China) are mines with complex hydrogeological conditions. In these mines, water confined in the roof strata affects the behavior of the rock and hence the safety risks associated with the mining activities [1]. The mines are located within the Ordos Basin, with the coal seams hosted within the Jurassic Yan'an Formation. This formation is positioned between the older Fuxian Formation below and younger Zhiluo Formation above. The Yan'an Formation has been divided stratigraphically into five

subunits, namely, Y1, Y2, Y3, Y4, and Y5. The most important coal seam in the Yan'an Formation for mining purposes is the 2-2 coal seam.

The mining of the 2-2 coal seam in the Yan'an Formation is affected by water stored in the overlying Zhiluo Formation and the section of the Yan'an Formation above this coal seam. The occurrence of the water in the overlying strata is irregular over short distances [2–5]. Rock burst prevention practices, such as roof water drainage for small coal pillars, have further complicated the ground stress environment of the gob-side roadway. In the gob-side roadways, in drained areas of a mine, head-on ejection of coal has occurred multiple times, some of which have resulted in injuries to mine workers.

Many scholars have explored the relationship between the stress transfer induced by borehole drainage (or water inrush) and the rock bursts in roadways not subject to current mining activity. Shu et al. [6, 7] proposed that roof drainage modifies the physicomechanical properties of aquifers, damaging them in the process. By using a method based on the principle of superposition for load analysis, they suggested that rock bursts could be induced by drainage through holes drilled during drive development (non-gob-side).

Li et al. [8–10] postulated that superposition between the step-up belt formed by drainage of confined water in the roof strata and the relatively greater bearing stress can lead to rock bursts. On this basis, they built a model for estimating roof confined water drainage and stress transfer. This model enabled them to show that the stress transfer could be caused by drainage. Using experimental methods, they discovered that water reduced the strength of the coal and argued that the weakening of the surrounding rock strength would increase the rock burst risk.

Wang et al. [11, 12] proposed a rock burst inducement mechanism dependent on "strong disturbance-drainage" in the high-intensity working face of the area of roof subject to drainage. They also developed models for estimating post-drainage and advanced bearing pressures, respectively. They tested their proposed inducement mechanism by carrying out field-based microseismic monitoring and numerical simulation. Based on the results of the studies, they proposed preventative measures for controlling the rate stoping development in the drained area.

The effect of roof drainage on rock bursts along a roadway and at a working face has also been investigated. However, gob-side driving differs from both solid entry driving, and working face stoping, in that gob-side entry driving, is carried out after stress redistribution. The stress redistribution could be attributed to the release of water pressure through drainage holes, or gob fissures. Gob-side entries are susceptible to rock bursts, and hence, the stress field characteristics of rock strata in close proximity to gob-side entries are of critical importance for rock burst hazard assessment [13, 14]. In addition, roof drainage, coal pillar width, coal pillar damage (the energy rate can be used to reflect the plastic failure of coal [15]), and roof fracture characteristics affect the nature of the stress field in rocks subject to gob-side entries [16–20].

References [6–12] have described how roof drainage-related stress in strata affects the occurrence of rock bursts in solid entry driving and stoping entries. However, they did not describe head-on coal bursts and rock bursts along roadways with small coal pillars. Furthermore, the ejection phenomena (e.g., spalling and rock bursts) that occur along the roadways with small coal pillars in other domestic mining areas have been rarely reported. In this context, research should be carried out to clarify the risks associated with the gob-side entry driving of small coal pillars subject to drainage.

This study used the elastic foundation beam model (based on the principle of load superposition) for roof drainage to analyze the changes to roof drainage stress during gob-side driving conditions. This paper also provides a description of how the stresses in the rock in these conditions can be assessed using a rock burst risk ranking for various roadway areas and introduces a rock burst reduction measure, namely, head-on large-diameter borehole placement to prevent (or mitigate) head-on-related rock burst risks.

2. Evolution of Roof Drainage Stress

The exploitation of coal seam resources causes the loss of groundwater [21]. On the damage of rock strata caused by drainage engineering for prevention and control of water inrush, Li et al. [8–10] focused their research on the effect of water on the lithology of coal. Shu, Wang et al., and Miao et al. [6, 22, 23] also examined the effect of water on the lithology of rocks. These studies showed that water played a major role in the weakening of coal and rocks. However, their conclusions were based on comparisons of the lithology of coal or rock samples before and after soaking in water. Zhao et al. used COMSOL Multiphysics software (version, COMSOL Inc., https://www.comsol.com/) to run simulations and model the damage and deformation caused by overburden and the loss of water from aquifers during mining. They found that seepage did not change the value of the rock parameters in the rock mechanics module [24]. Before drainage, a significant amount of time would have passed during which the nature of physicochemical reactions between the water and rock strata would have been relatively stable. The weakening of strata in this context differs from that taking place when dry sandstone is soaked in water, namely, during the relatively short periods typically associated with experiments. Therefore, in order to address the limitations associated with this modelling-based approach, we should take into account the weakening of rock physicomechanical properties by mining-induced drainage.

Stress transfer is essentially a result of movement in rock strata. The scope of drainage stress transfer and the degree of stress concentration are directly related to the movement in the strata subjected to the drainage. Before the mining of an adjacent working face in gob-side entry driving, the pattern and degree of stress distribution caused by drainage can be determined using the elastic foundation beam model. The analysis is based on values obtained for movement and the measured specific pressure drop induced by overburden drainage.

After roof water drainage, the roof stratum above the drained area (the medium-fine sandstone stratum in our case study) can be regarded as a double-clamped beam, the length of which is related to the distance of the stratum away from the drained stratum. That is, the longer the distance of the stratum away from the drainage stratum, the greater the length of the beam. The load applied on the double-clamped beam was determined by deducting the stress transferred by the underlying relatively weak stratum from the water pressure drop after drainage.

The disturbance-related stress induced by drainage is borne jointly by the rocks in and outside the area that has been drained. Before the working face is mined, boreholes are drilled for drainage purposes into the two aquifers (i.e., Zhiluo Formation and Yan'an Formation). The drained stratum is located outside the plastic zone of the roadway, with the stratum in the drained area treated as an elastomer. References [8, 12] also treat the stratum in the drained area as an elastomer [8, 12]. The load borne by the elastic bearing zone was assumed to be a uniformly distributed load σ_e, with the rocks in and outside the drained area equated to a continuously distributed Winkler foundation model. The overlying stratum was treated as a double-clamped beam [25, 26], as shown in Figure 1. A simplified three-component mechanical model, based on the characteristics of the rocks (a) in the drained area, (b) the rocks outside the drained area, and (c) the overlying stratum, is shown in Figure 2.

The origin of the coordinates O was located at the edge of the drained area. The coordinate system was set up using the exterior of the drained area as the positive x-axis and roof deflection function $w(x)$ as the unknown quantity, where σ_e denoted the uniformly distributed load borne by the overlying stratum, k_n denoted the response modulus of the foundation in the drained area, and k_w denoted the response modulus of the foundation outside the drained area.

According to the basic principles of elasticity mechanics, the relationship between the strain and stress borne by the rocks in the drained area can be expressed using the following formula:

$$\varepsilon = \frac{\sigma}{E_n}, \tag{1}$$

where E_n denoted the elastic modulus of the rocks in the drained area.

Following Winkler's hypothesis [27], the relationships between the roof deflection function $w(x)$ with load σ_e and foundation pressure $p(x)$ can be expressed as

$$\frac{\mathrm{EI}d^4w(x)}{dx^4} = \sigma_e - p(x), \tag{2}$$

where EI denotes the bending strength of a random beam section, E denotes the elastic modulus, and I denotes the sectional moment of inertia.

The deflection w of a random point on the foundation is directly proportional to the pressure p applied at this point:

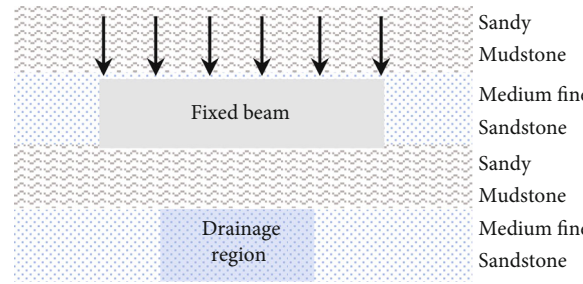

Figure 1: Fixed beam model of rock above drainage area.

$$k = \frac{p(x)}{w(x)}, \tag{3}$$

where k denotes the response modulus of the foundation, $p(x)$ denotes the specific pressure borne by the foundation, and $w(x)$ denotes the deflection value of the foundation.

The deflection equation for the overlying stratum in the drainage area can therefore be expressed as

$$\frac{\mathrm{EI}d^4w(x)}{dx^4} = \sigma_e - k_n w(x). \tag{4}$$

After defining the characteristic constant $\alpha = \sqrt[4]{k_n/EI}$, we have

$$\frac{d^4w(x)}{dx^4} + 4\alpha^4 w(x) = \frac{\sigma_e}{\mathrm{EI}}. \tag{5}$$

By solving the above equation, we obtain the following general solution:

$$\begin{aligned} w(x) = \sigma_e/k_n + d_1 e^{\alpha x}\cos(\alpha x) + d_2 e^{\alpha x}\sin(\alpha x) \\ + d_3 e^{-\alpha x}\cos(\alpha x) + d_4 e^{-\alpha x}\sin(\alpha x), \end{aligned} \tag{6}$$

where constants d_1, d_2, d_3, and d_4 are undetermined parameters, while the roof deflection equation $w(x)$ can be used to determine the boundary and continuity conditions. The stress values for corresponding positions can be calculated by using the elastic moduli k_n and k_w of the strata in and outside the drained area and the roof deflection equation.

$$\sigma = kw(x). \tag{7}$$

The relationship between the maximum deflection of the beam and the compressive deformation of the drainage stratum can be assigned to one of two patterns:

(1) The "M" stress distribution pattern when the maximum deflection of the beam is no greater than the compressive deformation of the drainage stratum (Figure 3(a))

(2) The irregular wave-like stress distribution pattern when the theoretical maximum deflection of the

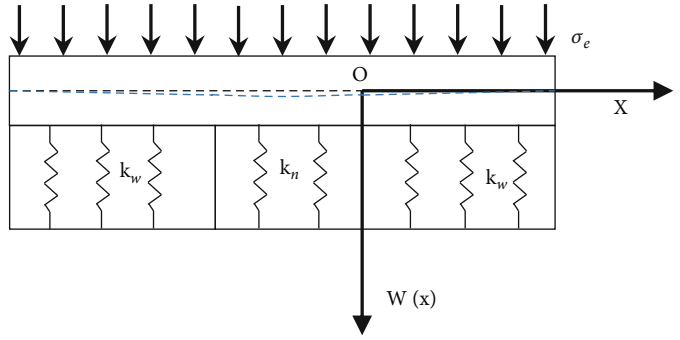

Figure 2: Mechanical model of roof in drainage area.

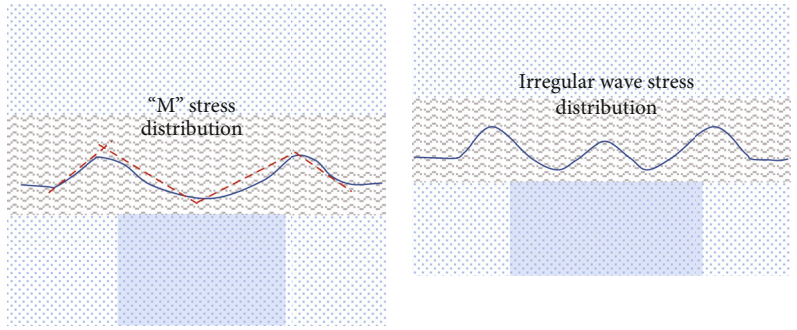

Figure 3: Schematic diagram of stress distribution of different drainage zone widths.

beam is greater than the compressive deformation of the drainage stratum (Figure 3(b))

We propose that when the theoretical maximum deflection of the beam is greater than the compressive deformation of the drainage stratum, the stratum in the middle of the drained area can still support the overlying stratum, giving rise to stress transfer similar to that in the case of gob compaction. In certain conditions, the stress restoration zone in Figure 3(b) may form a platform-type stress distribution (Figure 3(b)). In this paper, a drainage stress transfer model is built using the "M" stress distribution pattern as an example.

Before drainage, the vertical stress is uniformly distributed in the water-rich stratum. After drainage, the decline in the water pressure in the drained area weakens its supporting effect in the overlying stratum and causes the stratum above the drained area to subside. As a result, the vertical stress in the drained area is transferred outwards, giving rise to a low-stress zone in the drained area and a high-stress zone adjacent to it (Figure 4).

The elevated stress zone formed in this way affects the distribution of stress in the coal in the drained area. The path of stress transfer, indicated by the green-dotted arrow in Figure 4, shows the downward transfer of stress in accordance with a certain stress dispersion angle. The stress increment curve, indicated by the green solid curve in Figure 4, represents the change in stress in the coal seam.

These results are consistent with the findings of earlier studies. We therefore concluded that the morphology of the edge of the drained area and the relative spatial relationship between the roadway and the edge of the drained area affected the level

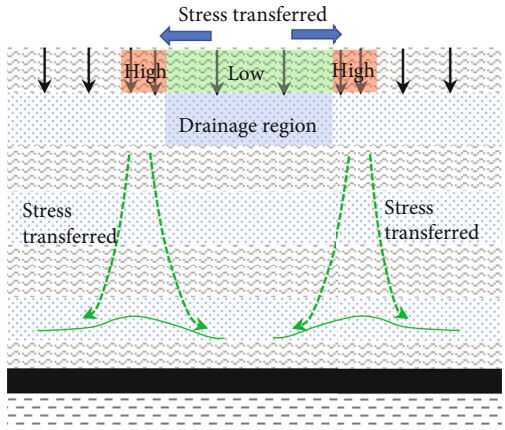

Figure 4: Stress transfer model after drainage.

of rock burst risk caused by entry driving. This finding was corroborated by (1) the concentration of microseismic events in the concave angle area of the drained area (reference [12]) and (2) the concentration of microseismic events in the driving region parallel to the edge of the drained area (Figure 5).

3. General Relationship between the Drained Area and the Gob-Side Entry Area

The overburdens at the gob boundary rotate and subside form a structure supported by one fulcrum on the coal wall and another on the gangue. The multilayer spatial structure

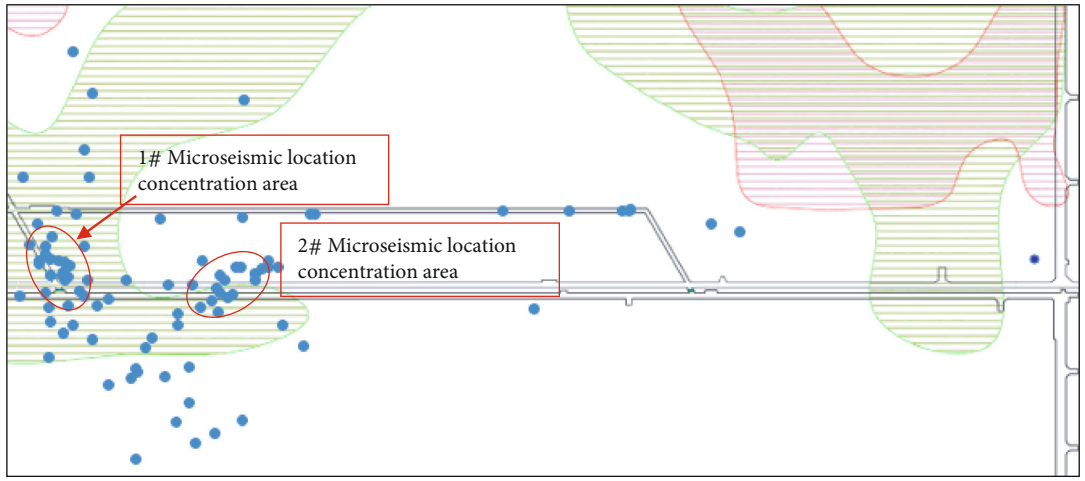

Figure 5: Distribution of microseismic events during the period of the 2202 auxiliary transport roadway excavation.

produces a stress increment in coal via the fulcrum on the coal wall [28].

The positional relationship between the drained area and the gob-side entry has three potential scenarios:

(1) The gob-side entry is located in the postdrainage low pressure zone

(2) The gob-side entry is located in the drained area with a pressure gradient between the drained (low pressure) and undrained (higher pressure) areas (i.e. coal seam)

(3) The gob-side entry is unaffected by the drained area

After the drained area has been subjected to mining activity at the working face, the fissures in the fissure zone become drainage channels. While the elastic foundation beam model is no longer applicable to a drained area affected by mining, there is no fundamental change in the stress transfer laws in the drained area. That is, a low-stress zone still takes shape in the drained area, and a high-stress zone still forms at the boundary of the drained area [11].

After mining activity has taken place at the working face, the lateral stress present is as shown by the black-dotted curve in Figure 6. When the gob-side entry is in the postdrainage low pressure zone, the stress originally acting on the gob-side driving region on the solid coal wall side is transferred by the drained area to the boundary of the drained area. As a result, the stress level at the gob-side driving position drops below the lateral stress experienced in the undrained area, as indicated by the solid black curve in Figure 6.

In contrast, when the gob-side entry is in the postdrainage zone with a pressure gradient, the stress originally acting on the postdrainage low pressure zone is transferred by the drained area, partially to the gob-side driving region. This partial stress transfer produces a stress increment in the gob-side driving region, causing the stress level of the gob-side driving region to increase, as indicated by the solid black curve in Figure 7.

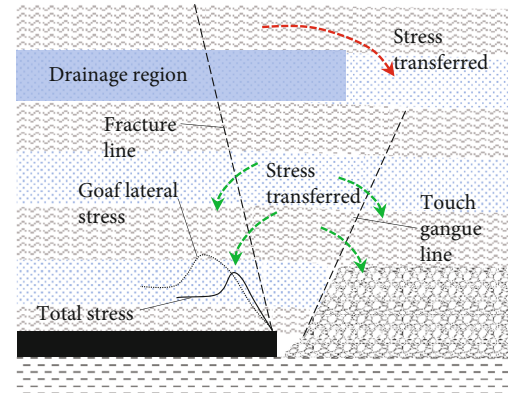

Figure 6: Stress evolution of roadway along goaf located in drainage depressurization area.

4. Mechanism and Criteria for Head-On Rock Bursts

Head-on rock bursts are closely related to the physicomechanical properties and stress state of coal. Roof drainage affects the stress state in the coal. This section describes the effect of roof drainage on the stress state and the stress-induced mechanism for head-on rock bursts in gob-side driving due to roof drainage.

4.1. Rock Burst Risk Ranking for Various Roadway Areas. Regardless of chambers or crosscuts, the stress increment concentration coefficient for the effect of the gob on gob-side entry driving was consistent. If the stress increment concentration coefficient is λ, the stress at the position where the roadway is located becomes

$$\sigma_1 = (1 + \lambda)\gamma H, \tag{8}$$

where σ_1 denotes the stress in the surrounding rock due to gob-side entry driving; λ denotes the stress increment concentration coefficient for the surrounding rock produced by the gob-side entry driving, set as 0.5 (i.e., lateral stress concentration coefficient = 0.3 and driving stress

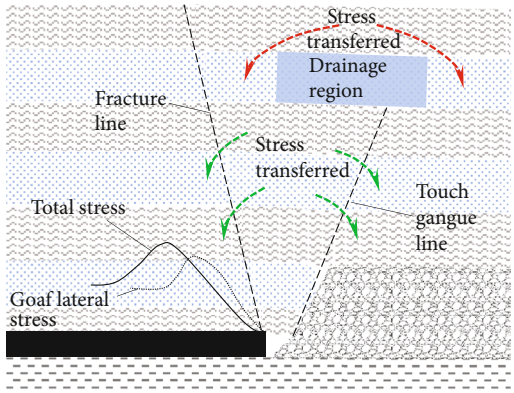

Figure 7: Stress evolution of roadway along goaf located in drainage pressurization area.

concentration coefficient = 0.2); γ denotes the bulk density of the stratum, set as 2,500 kg/m^3; and H denotes the burial depth of the roadway.

When gob-side entry driving is affected by roof drainage, the specific effect varies with the positional relationship between the driving face and the drained area. We assumed that the stress increment concentration coefficient and stress reduction concentration coefficient of the drained area had the same value and that the stress concentration coefficient was z. Driving in the water-rich zone (WRZ), driving in the water-poor zone (WPZ), and driving along the water-rich zone boundary (WRZB) are affected by roof drainage stress redistribution and gob lateral stress in different ways. In the case of driving along the WRZB, the effects of roof drainage stress redistribution and gob lateral stress are mutually enhanced via superposition. Driving in the WPZ is affected by gob lateral stress alone. In the case of driving in the WRZ, roof drainage stress redistribution and gob lateral stress are mutually weakened via superposition, and roof drainage stress redistribution weakens the effect of gob lateral stress on the gob-side driving roadway.

$$\sigma_2 = (1 + \lambda + z)\gamma H, \tag{9}$$

$$\sigma_3 = (1 + \lambda - z)\gamma H, \tag{10}$$

where σ_2 denotes the stress in the surrounding rock in the gob-side entry driving at the edge of the drained area, σ_3 denotes the stress in surrounding rock in the gob-side entry driving in the drained area, and z denotes the stress increment concentration coefficient for surrounding rock produced by drainage, with a mean value set at 0.2 [7].

The rock burst risks for the three roadway areas can be ranked in descending order according to the stress levels in different regions of the areas subject to gob-side driving, with the stress at the edge of the drained area > the undrained area > the drained area.

Due to the superposition of roof drainage stress and gob lateral stress, the stress level exceeds the stress threshold at which rock bursts occur in coal, at the working face of areas subject to gob-side driving. Rock bursts therefore occur in the areas where gob-side driving takes place.

4.2. Stress Criterion for Head-On Rock Bursts. For the prediction of rock burst hazards in mining engineering, "coal stress >1.5 times the integrated compressive strength" has been used as the stress threshold for assessing the level of rock burst hazard [29].

There is obvious zonation based on mining stress in the head-on direction of drive development, namely, a destressing zone (simulation results indicate that close to the coal wall, the stress vertical to the axial direction of the roadway is less than 4 MPa), a stress concentration zone, and an in situ stress zone [30]. Head-on ejection occurs near the head-on coal wall, within the destressing zone. The results in our study indicate that the widely used threshold value of 1.5 times the integrated compressive strength of the rock is probably not suitable for use as the critical stress for assessing the likelihood of a rock burst occurring near the coal wall.

Ejection is similar to tunnel rock bursts. The index used to predict rock bursts in tunnels is based on the ratio of rock uniaxial compressive strength to ground stress. That is, when the ratio is greater than 5, no rock burst occurs; when the ratio is between 2.5 and 5, mild or moderate rock bursts occur; and when the ratio is less than 2.5, severe rock bursts occur [31]. That is to say, the stress-strength ratios of 0.2 and 0.4 are taken as thresholds for assessing the level of the rock burst hazard (i.e., no rock burst hazard, mild to moderate rock burst hazard, and severe rock burst hazard). There are also studies that use 0.15, 0.2, 0.3, or 0.34 as the threshold value [32].

In uniaxial or triaxial compression tests on coal samples, the stresses under which ejection occurs generally exceed 0.6 σ_c. In a total of 15 tests, the stresses have exceeded 0.6 σ_c in 13 tests (with 0.25 σ_c and 0.45 σ_c each occurring once) [33–36].

On the basis of the above analysis, the stress criterion for assessing the presence of ejection near the coal wall can be obtained from outburst susceptibility tests, including (1) the occurrence (or not) of coal ejection during loading and (2) the critical stress for the occurrence of ejection.

5. Engineering Cases

5.1. Engineering Background. The 2-2 coal seam is the primary mineable coal seam in most mines in the Uxin Banner. The safe and efficient mining of the 2-2 coal seam offers an important guarantee for mine output. When the auxiliary haulage roadway of the 2202 working face of a mine is driven at the edge of the drained area, there can be frequent coal bursts, and drill rods can jam in destressing boreholes and drill cutting holes. In particular, in the case of driving within II in Figure 8, coal ejection occurs, accompanied by head-on coal ejection, coal bursts, and massive amounts of coal dust.

The auxiliary haulage roadway of the 2202 working face is the roadway for gob-side driving, located 5 m away from the 2201 gob and 300 m away from the 2202 belt conveyor haulage roadway. At a site 80 m away from the auxiliary haulage roadway of the 2202 working face, there is an auxiliary haulage roadway for the 2201 working face, which is

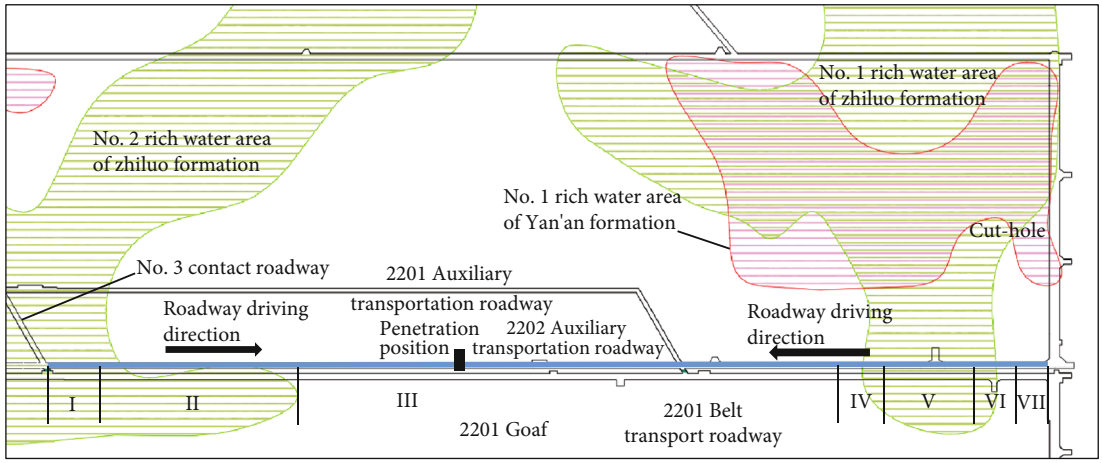

Figure 8: Spatial relationship of the roadway (the blue line is 2202 auxiliary transport roadway).

Table 1: Composite columnar section of the 2202 working face.

Strata	Thickness (m)	Comment
Medium-fine sandstone	12.91	The relative water-rich anomaly region of the Zhiluo formation
Sandy mudstone	12.45	
Medium-fine sandstone	13.56	
Sandy mudstone	13.90	
Medium-fine sandstone	11.56	The relative water-rich anomaly region of the Yan'an formation
Sandy mudstone	6.87	
2-2 coal seam	6.50	

connected via the #3 crosscut. The crosscut intersects with the auxiliary haulage roadway of the 2202 working face.

The coal seam of the 2202 working face has a floor elevation of 516-521.3 m (average = 518.7 m) and a ground elevation of 1,249.8-1,250.4 m (average 1,250.1 m). The mean burial depth of the working face is 731.4 m. The coal seam has a simple structure and is unaffected by faults, folds, or other geological structures. The dip angle of the coal seam is 0-4° (average = 2°).

Distribution of roof water: the relatively water-rich strata of the Yan'an and Zhiluo Formations are located above the 2-2 coal seam, as shown in Figure 8. The area filled with green horizontal lines is the relatively water-rich Zhiluo Formation, while that filled with red horizontal lines is the relatively water-rich Yan'an Formation. Entry driving proceeds at one end from #3 crosscut towards the open offcut and at the other end from the open-off cut towards #3 crosscut, as illustrated in Figure 8. Depending on the specific effect of the drained area in the Zhiluo Formation on stress in driving, the spatial relationship between the drained area and driving is divided into four types (i.e., driving parallel to the edge of the drained area, driving vertically to the edge of the drained area, driving in the drained area, and driving in the undrained area), which are connected at the positions indicated in Figure 8.

As shown in Figure 8, on the basis of the relationship between entry driving and the drained area (with the point of intersection between the 2202 auxiliary haulage roadway and the #3 crosscut being the origin), the roadway is divided into seven areas: I (0-45 m), II (45-250 m), III (250-782 m), IV (782-842 m), V (842-913 m), VI (913-973 m), and VII (973-996 m). To be more specific, I and V involve driving in the drained area; II involves driving parallel to the edge of the drained area; III and VII involve driving in the undrained area; and IV and VI involve driving vertically to the edge of the drained area.

The composite columnar section is shown in Table 1. Above the 2-2 coal seam, there is an intercalated sequence of sandy mudstone and medium-fine sandstone. The roof of the 6.5 m thick coal seam is a 6.87 m thick layer of sandy mudstone, and the basic roof is a 11.56 m thick layer of medium-fine sandstone. The relatively water-rich Yan'an Formation is located in the medium-fine sandstone layer of the basic roof. When the 2202 auxiliary haulage roadway is driven between the #3 crosscut and the open-off cut, the relatively water-rich Yan'an Formation is not involved. The relatively water-rich Zhiluo Formation is located 58.34 m above the 2-2 coal seam. The height of the diversion fissure zone of the mine is 21 times the mining height, namely, $6.5\,\text{m} \times 21 = 136.5\,\text{m}$, which is far greater than the distance from the relatively water-rich Zhiluo Formation in the mine to the 2-2 coal seam.

5.2. Rock Burst Risk Prediction for Gob-Side Entry. By analyzing the stress transfer of the drained area and the spatial relationship between the drained area and the gob, we were

able to predict that there are different rock burst risks associated with the different areas in the driving of the 2202 auxiliary haulage roadway. The roadway area can be divided into four areas, in order to predict rock burst risk, namely, drives in the drained area, drives in the undrained area, vertical drives to the edge of the drained area (i.e., stopes), and drives parallel to the edge of the drained area.

The driving of the 2202 auxiliary haulage roadway is mainly affected by roof drainage-related stress redistribution, gob lateral stress, and coal cutting in the 2201 auxiliary haulage roadway. The distribution of the gob lateral stress field is related to the distance away from the gob. The 2201 gob and the 2201 auxiliary haulage roadway exert the same effect on the driving of various areas of the 2202 auxiliary haulage roadway. In areas where coal pillar width varies due to chambers or crosscuts, gob lateral stress has a differential effect on the driving of the 2202 auxiliary haulage roadway. In entry driving, microseismic events are triggered in areas affected by chambers or crosscuts.

The roadway parallel to the edge of the drained area is located along the length of the high-stress zone. Compared with roadways driven perpendicular to the edge of the drained area (which only passes through the high-stress zone), roadways driven parallel to the edge of the drained area are more dangerous. In combination with the analysis in Section 3, the seven areas can be ranked as follows in descending order of rock burst risk, namely, II > IV, VI > III, VII > I, and V.

5.3. Field Monitoring. Many microseismic events are observed in the driving of the 2202 auxiliary haulage roadway. In particular, it is difficult to identify the distribution of microseismic events in the #1 and #2 seismic focus concentration areas marked in Figure 5 Microseismic events occurring in the driving of the 2202 auxiliary haulage roadway are screened, while those with an energy level above 10^4 joules are marked on the mining engineering plan, as shown in Figure 5.

The microseismic events shown in Figure 5 are concentrated in two areas. The areas marked by red ellipses are the #1 and #2 seismic focus concentration. The emergence of the #1 seismic focus concentration area is mainly attributable to the #3 crosscut. In the opening and initial driving stage of the 2202 auxiliary haulage roadway, driving disturbance affects the #3 crosscut, resulting in microseismic focus concentration in the vicinity of the #3 crosscut. The emergence of the #2 seismic focus concentration area is due to roof drainage, especially in the overlapping area between the edge of the drained area and the roadway.

While the distribution of microseismic events indicates the degree of roadway disturbance, it is also useful to analyze the information collected from microseismic monitoring work. For this statistical analysis, we selected the microseismic events that were recorded within 40 m, either side of a 10 segment of the roadway. Microseismic energy describes the statistical distribution of individual events in relation to the amount of energy released. Descriptive statistics were calculated for these microseismic events. In Figures 9 and 10, the point of intersection between the 2202 auxiliary haulage roadway and the #3 crosscut is taken as the origin and the open-off cut direction of the working face as the positive x-axis.

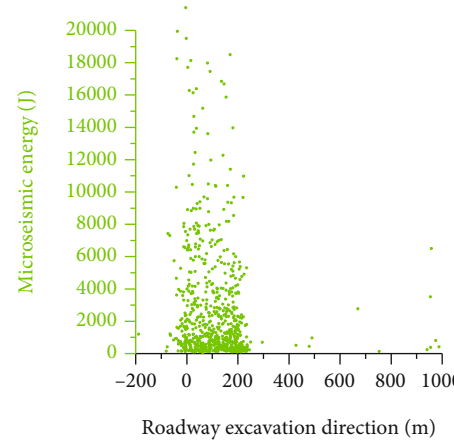

Figure 9: The distribution of microseismic energy along roadway excavation direction.

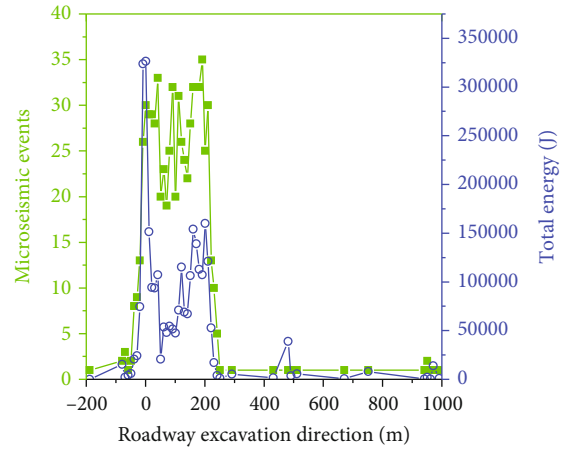

Figure 10: The distribution of the number of microseismic events and total energy along roadway excavation direction.

The concentrated distribution of individual event energy, event count, and total energy was observed between -40 and 240 m, with both individual event energy and event count displaying a uniform distribution. However, the distribution of total energy displayed obvious regularities. At 0 m, there was a maximum peak in total energy, which could be attributed to the roadway opening having disturbed the original balance of the rock surrounding the #3 crosscut. From 50 to 100 m, there was a dip in the magnitude of the total energy values. This implied that the area was unaffected by the #3 crosscut and only slightly affected by proximity to the edge of the drained area. From 50 to 210 m, there was an obvious rise in the total energy released by microseismic events, as the edge of the drained area gradually approached the roadway, with entry driving affected by the edge of the drained area to an increasingly large degree. From 210 to 240 m, both event count and total energy decline rapidly, and entry driving is separated from the edge of the drained area and enters the drained area.

5.4. Monitoring and Destressing. Head-on monitoring methods include the monitoring of microseismic events and drill cutting. Large-diameter boreholes were used for distressing purposes. Monitoring plans and destressing measures were implemented in the field to effectively mitigate the occurrence of stress release-related events, such as rock bursts.

5.4.1. Monitoring Plans

(1) Microseismic Monitoring. The microseismic monitoring system adopted for the mine could cover all the mining areas of the mine. In the driving of the 2202 auxiliary haulage roadway, analysis was performed on all microseismic monitoring data related to roadway driving, including microseismic frequency, energy, their distribution characteristics, and patterns of variation.

(2) Drill Cutting Monitoring. Two boreholes (with a pitch of 1 m and a diameter of 42 mm) were arranged head-on and drilled vertically into the coal wall. Drill cutting holes were 15 m in depth. The safe distance for drill cutting monitoring was 5 m.

5.4.2. Destressing Measures. Local destressing measures generally include blasting destressing, injection/hydraulic fracturing, and large-diameter borehole destressing. Large-diameter boreholes, characterized by simple operation and strong adaptability to head-on operating conditions during driving, were selected for head-on distressing purposes. The boreholes used for the head-on destressing of the driving face had a diameter of 150 mm and a depth of ≥30 m and were located at least 0.5 m above the roadway floor. Cyclic construction was carried out, with the belt of destressing protection at least 10 m in width.

6. Conclusions

This paper developed a model for assessing the rock burst hazard induced by roof drainage in gob-side driving. This model for the drained stratum overburden was based on the theory for a continuously distributed Winkler elastic foundation. It was used to analyze the link between the relatively water-rich anomalies in the Yan'an and Zhiluo formations and the lateral stress field of the stope adjacent to gob-side entry driving-related activities. The model could be used to describe the mechanism by which the composite stress in the water-bearing stratum triggers head-on rock bursts during drive development.

(1) According to calculations based on the theory of a continuously distributed Winkler elastic foundation, a zone with a pressure gradient develops at the edge of the drained area postdrainage, and a low pressure zone forms in the drained area

(2) The spatial relationship between the drained area and the gob-side entry driving generally covers the following scenarios: the gob-side entry is located in the postdrainage low pressure zone; the gob-side entry is located in the postdrainage zone with a pressure gradient; or the drained area affects the stress state, level of rock burst risk, and dynamic manifestations of the driving region

(3) By combining the characteristics of the ejections observed in the mines, with the ejections observed in the laboratory, it can be concluded that the stress criteria for assessing the occurrence of ejection phenomena should include the following:

   (a) The occurrence (or not) of coal ejection during loading

   (b) The critical stress threshold required for an ejection to be triggered

(4) On the basis of the spatial relationship between the drained area and the drive for the 2202 auxiliary haulage roadway, roadway drives can be divided into seven areas and four types. The driving region parallel to the edge of the drained area constitutes a key area for the prevention of head-on rock bursts. In this scenario, if the monitoring of microseismic events and drill cutting are combined with the implementation of head-on large-diameter borehole destressing measures, mining should be able to take place safely

While drainage is the external cause of ejections (e.g., rock bursts), the physicomechanical properties of coal represent the internal cause. In future research, we will explore how the physicomechanical properties of coal affect rock burst phenomena in the Uxin Banner.

Data Availability

Data available on request.

Conflicts of Interest

The authors declare that there is no conflict of interest regarding the publication of this paper.

Acknowledgments

This research is supported by the National Natural Science Foundation for Young Scientists of China (Grant No. 52004004).

References

[1] B. C. Shi and Y. Li, "Inner Mongolia Coal Mine Safety Supervision Bureau Ordos Supervision Branch," in *How to Break the Dilemma of "Rock Burst"*, China Coal News, 2021.

[2] J. Yang and X. Ding, "Dewatering and depressurizing effect of roof water in deep buried coal seam of Shaanxi and Inner Mongolia contiguous area," *Safety in Coal Mines*, vol. 34, no. 6, pp. 35–39, 2013.

[3] X. Y. Liang, J. Yang, and Z. G. Cao, "Characteristics and sedimental control of mine water outflow in Hujirt mining area," *Coal Geology & Exploration*, vol. 48, no. 1, pp. 138–144, 2020.

[4] G. Chen, *Study on the Deep Transfer and Storage Mechanism of Mine Water in the Eastern Margin of Ordos Basin*, China University of Mining and Technology, 2020.

[5] Y. H. Wang, *Research on Characteristics of Water Gushing and Mining Technology in Xiaojihan Coal Mine*, China University of Mining and Technology, 2019.

[6] C. X. Shu, *The Mechanism and Prevention of Rock Burst Occurrence at Water-Rich Working Face of Depth Mine in the Adjacent Area of Shaanxi and Inner Mongolia*, University of Science and Technology Beijing, 2018.

[7] C. X. Shu, F. X. Jiang, and Q. D. Wei, "Mechanism and treatment of rockburst inducedby drainage in roadways in deep coal mines," *Journal of Mining & Safety Engineering*, vol. 35, no. 4, pp. 780–786, 2018.

[8] D. Li, *Mechanism and Control Techniques of Rockburst Disasters in Deep Mines with Thick Topsoil and Confined Water-Bearing Roofs*, University of Science and Technology Beijing, 2018.

[9] D. Li, F. X. Jiang, C. W. Wang, Z. J. Tian, Y. Wang, and J. H. Liu, "Study on the mechanism of rockburst induced by water inrush from deep," *Chinese Journal of Rock Mechanics and Engineering*, vol. 37, no. S2, pp. 4038–4046, 2018.

[10] D. Li, F. X. Jiang, Y. Chen et al., "Mechanism of rockburst induced by "dynamic-static" stress effect in water-rich working face of deep well," *Chinese Journal of Geotechnical Engineering*, vol. 40, no. 9, pp. 1714–1722, 2018.

[11] B. Wang, S. T. Zhu, Q. D. Wei, Y. S. Gu, Z. C. Li, and B. Zhang, "Mechanism and prevention measures of rock burst rapid mining face of roof drainage area," *Safety in Coal Mines*, vol. 51, no. 7, pp. 205–209, 2020.

[12] B. Wang, F. X. Jiang, S. T. Zhu et al., "Investigating on the mechanism and prevention of rock burst induced by high intensity mining of drainage area in deep mines," *Journal of China Coal Society*, vol. 45, no. 9, pp. 3054–3064, 2020.

[13] Y. H. Cheng, F. X. Jiang, Z. F. Hu, and J. K. Lin, "Prevention and control of coal burst on gob-side entry in deep coal seam with fully mechanized sublevel caving mining," *Chinese Journal of Rock Mechanics and Engineering*, vol. 35, pp. 3000–3007, 2016.

[14] Z. Q. Wang, P. Wang, L. Shi et al., "Research on prevention of rock burst based on stress analysis of surrounding rock of gob-side entry," *Journal of China University of Mining and Technology*, vol. 49, no. 6, pp. 1046–1056, 2020.

[15] Y. Xue, J. Liu, P. G. Ranjith, Z. Zhang, F. Gao, and S. Wang, "Experimental investigation on the nonlinear characteristics of energy evolution and failure characteristics of coal under different gas pressures," *Bulletin of Engineering Geology and the Environment*, vol. 81, no. 1, p. ???, 2022.

[16] J. F. Pan, S. H. Liu, J. M. Gao, X. K. Sun, Y. X. Xia, and Q. Wang, "Prevention theory and technology of rock burst with distinguish dynamic and static load sources in deep mine roadway," *Journal of China Coal Society*, vol. 45, no. 5, pp. 1607–1613, 2020.

[17] Y. D. Jiang, H. H. Song, Z. Q. Ma, B. J. Ma, and L. T. Gao, "Optimization research on the width of narrow coal pillar along goaf tunnel in tectonicstress zone," *Journal of China Coal Society*, vol. 43, no. 2, pp. 319–326, 2018.

[18] L. I. Xue-Hua, L. Shun, Y. A. O. Qiang-Ling, and Q. U. Qun-Di, "Control principle and its application of rock burst in roadway driving along goaf with outburst-proneness surrounding rocks," *Journal of Mining & Safety Engineering*, vol. 29, no. 6, pp. 751–756, 2012.

[19] G. Han, L. M. Dou, Y. Zhang, X. D. Li, Q. Wang, and Y. L. Lyu, "Influence mechanism and prevention technology of dynamic manifestation of roadway along goaf," *Journal of Mining & Safety Engineering*, vol. 38, no. 4, pp. 730–738+748, 2021.

[20] J. Wang, J. Q. Jiang, G. B. Li, and H. Hu, "Exploration and numerical analysis of failure characteristic of coal pillar under great mining height longwall influence," *Geotechnical and Geological Engineering*, vol. 34, no. 2, pp. 689–702, 2016.

[21] Y. Xue, J. Liu, X. Liang, S. Wang, and Z. Ma, "Ecological risk assessment of soil and water loss by thermal enhanced methane recovery: numerical study using two-phase flow simulation," *Journal of Cleaner Production*, vol. 334, article 130183, 2022.

[22] Y. L. Wang, J. X. Tang, J. Jiang, Z. Y. Dai, and G. J. Shu, "Mechanical properties and parameter damage effect of malmstone under chemical corrosion of water-rock interaction," *Journal of China Coal Society*, vol. 42, no. 1, pp. 227–235, 2017.

[23] S. J. Miao, M. F. Cai, and D. Ji, "Damage effect of granite's mechanical properties and parameters under the action of acidic solutions," *Journal of China Coal Society*, vol. 41, no. 4, pp. 829–835, 2016.

[24] C. Zhao, D. Jin, H. Wang, Q. Wang, S. Wang, and Y. Liu, "Construction and application of overburden damage and aquifer water loss model in medium-deep buried coal seam mining in Yushen mining area," *Journal of China Coal Society*, vol. 44, no. 7, pp. 2227–2235, 2019.

[25] Q. S. Li and C. Zhang, "Damage conduction model of high intensity mining in western mining area based on conservation of mining space and its application," *Journal of Mining & Safety Engineering*, vol. 38, no. 1, pp. 1–8, 2021.

[26] H. Y. Pan, S. G. Li, T. W. Zhang, and H. F. Lin,, "Composite key stratum module of Winkler foundation and its mechanical properties," *Journal of Central South University (Science and Technology)*, vol. 43, no. 10, pp. 4050–4056, 2012.

[27] Y. Q. Long, *Calculation of Beam on Elastic Foundation*, People's Education Press, Beijing, 1981.

[28] H. Shi and F. X. Jiang, "Study on abutment pressure rule of overlying strata spatial structures based on microseismic monitoring," *Chinese Journal of Rock Mechanics and Engineering*, vol. 27, pp. 3274–3280, 2008.

[29] F. X. Jiang, C. X. Shu, and C. W. Wang, "Impact risk appraisal of stope working faces based on stress superinposition," *Chinese Journal of Rock Mechanics and Engineering*, vol. 34, no. 12, pp. 2428–2435, 2015.

[30] S. H. Longyong, W. A. Kai, Q. I. Qingxin, and Z. H. Lang, "Stress field evolution characteristics and coal-gas outburst hazard evaluation model of the heading face in coal roadway," *Journal of Mining & Safety Engineering*, vol. 34, no. 2, pp. 259–267, 2017.

[31] Y. B. Li, *Road Tunnel Brittle Rock Burst Mechanism and Simulation Research*, University of Science and Technology Beijing, 2015.

[32] J. J. Zhang and B. J. Fu, "Rockburst and its criteria and control," *Chinese Journal of Rock Mechanics and Engineering*, vol. 27, no. 10, pp. 2034–2042, 2008.

[33] J. Lu, G. Z. Yin, H. Gao et al., "True triaxial experimental study of disturbed compound dynamic disaster in deep underground coal mine," *Rock Mechanics and Rock Engineering*, vol. 53, no. 5, pp. 2347–2364, 2020.

[34] J. Y. Fan, D. Y. Jiang, Z. H. Ouyang, T. Yang, J. Chen, and W. H. Liu, "Material-instability rock burst criteria based on the theory of strain gradient plasticity," *Journal of China Coal Society*, vol. 43, no. 11, pp. 2959–2966, 2018.

[35] D. W. Yin, S. J. Chen, W. B. Xing, D. M. Huang, and X. Q. Liu, "Experimental study on mechanical behavior of roof-coal pillar structure body under different loading rates," *Journal of China Coal Society*, vol. 43, no. 5, pp. 1249–1257, 2018.

[36] X. B. Wang, W. T. Hou, Y. S. Pan, and W. Dong, "Experiments of strain localization processes of coal speciments in uniaxial compression based on the digital image correlation method," *Journal of China Coal Society*, vol. 43, no. 4, pp. 984–992, 2018.